ACS EARTH AND SPACE CHEMISTRY

http://pubs.acs.org/journal/aesccq

Article

Theoretical Characterization of the High Pressure Nonclathrate CO_2 Hydrate

Fernando Izquierdo-Ruiz,* J. Manuel Recio, and Olga Prieto-Ballesteros

Cite This: https://dx.doi.org/10.1021/acsearthspacechem.0c00198

Read Online

ACCESS | Metrics & More | Article Recommendations | Supporting Information

ABSTRACT: On the basis of results from exhaustive first-principles simulations, we report a thorough description of the recently identified high pressure phase of the CO_2 hydrate, and provide an estimation of the transition pressure from the *sI* low pressure phase to the C_0 high pressure (HP) phase around 0.6 GPa. The vibrational properties calculated here for the first time might be useful to detect this HP structure in extraterrestrial environments, such as the Jupiter ice moons. Interestingly, we also find that CO_2 gas molecules are quasi-free to diffuse along the helical channels of the structure, thus allowing the interchange of volatiles across a solid icy barrier. Taking into account its density and comparing it with other substances, we can estimate the naturally occurring zone of this CO_2@H_2O HP phase within a giant ice moon such as Ganymede. Other potential planetary implications that all of the found properties of this hydrate might have are also discussed.

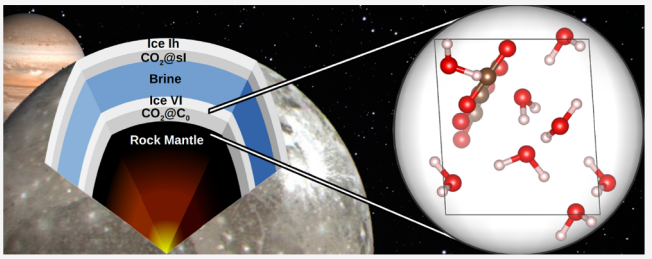

KEYWORDS: *ab initio calculations, high pressure, planetary science, phase transition, clathrates, hydrates, Ganymede*

1. INTRODUCTION

Clathrate hydrates are of primary importance in a variety of fields, from life sciences to planetology, and constitute a natural resource in the energy industry. These crystalline compounds accommodate guest molecules (usually of a nonpolar gas) within the framework of a tridimensional host web of water cages or channels. Although it ultimately depends on the nature of the guest molecule, clathrate hydrates generally need high pressure and low temperature to be stable. Pressure and temperature stability ranges are wide, displaying pressure-induced phase transitions between the main types of known clathrate hydrate structures: cubic *sI* and *sII*, hexagonal *sH*, and FIS (filled ice structure). The study of the high pressure (HP) phases of these clathrates is particularly relevant in planetary geophysics applications. Giant moons, such as Ganymede or Titan, show evidence of having deep internal water-rich layers in several phases, including liquid ones.[1] Some structural models indicate that liquid layers constitute planetary oceans squeezed between different phases of water ice, which might be under pressures up to 1 GPa. It is proposed that methane HP clathrates can be present in Titan below its ocean.[2] Similarly, if CO_2 is present within icy bodies like Ganymede or Pluto, it should form HP clathrate hydrates as well.[3,4] Their physicochemical properties, different from those of water ice phases, determine the thermal state, structure, and dynamics of these planetary objects.

Knowledge of basic structural and energetic behavior has been well established for CO_2 *sI* clathrate hydrates (see, for example, refs 5, 6, and references therein). However, in contrast with the number of experimental and theoretical studies on methane hydrate clathrates, the high pressure FIS phase has received less attention in the past. Methane hydrates have had a much more prominent focus earlier. Both the low and high pressure phases have been experimentally[7,8] and theoretically[9−11] described and are better known.[12] However, there have been new studies trying to characterize and interpret the high pressure behavior of CO_2 hydrates[4,13,14] and the kinetics of its formation,[15,16] but the high pressure phase of CO_2@H_2O has not been determined until recently.[17]

Our aim in this article is to thoroughly characterize the high pressure structure of this CO_2 hydrate evaluating short- (vibrational) and long-range (translational) atomic displacements, gas saturation stability regimes, its pressure−density equation of state (EOS) and the transition pressure from the well-known *sI* low-pressure structure. All the calculated data allow us to discuss potential warm and cold scenarios for the subsurface structure of Ganymede.

The article is organized in four more sections. Next, a brief summary of the computational details are presented. In Section 3, we analyze the calculated properties of the high pressure phase including different structural alternatives, the EOS, the

Special Issue: Materials of the Universe: The Final Chemical Frontier

Received: July 20, 2020
Revised: September 30, 2020
Accepted: October 16, 2020

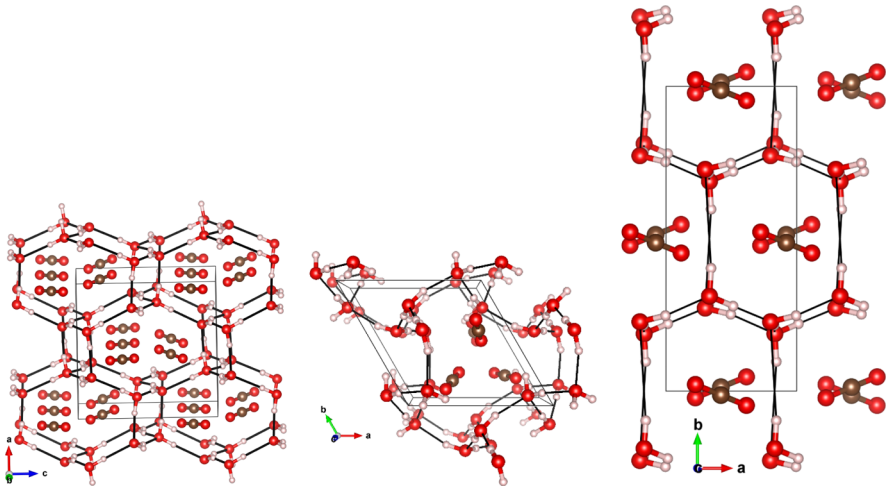

Figure 1. Optimized geometries of the possible structures of the CO_2 hydrate at high pressure. From left to right: Structures *A*, *B*, and *C*.

Table 1. Projected Views of the Optimized Lattice Parameters of the Three Potential Structures Proposed for the High-Pressure CO_2 Hydrate

structure	n_{H_2O}	n_{CO_2}	*a*	*b*	*c*	α	β	γ	*V* (Å^3)
empty *A*	8	0	7.92	4.53	7.83	90°	90°	90°	280.7
1 CO_2 *A*	8	1	8.61	4.45	7.49	88°	90°	90°	286.5
2 CO_2 *A*	8	2	8.63	4.46	7.45	93°	90°	90°	286.3
3 CO_2 *A*	8	3	9.05	4.64	7.59	92°	91°	97°	316.2
4 CO_2 *A*	8	4	9.03	4.79	7.29	90°	90°	90°	315.3
empty *B*	6	0	6.10	6.10	5.80	90°	90°	120°	187.3
1 CO_2 *B*	6	1	6.08	6.06	5.97	95°	86°	119°	192.0
2 CO_2 *B*	6	2	6.24	6.31	6.24	90°	91°	122°	208.7
3 CO_2 *B*	6	3	6.55	6.55	7.25	90°	90°	120°	269.0
B (exp[a])	6	1.69	6.2753	6.2753	6.2988	90°	90°	120°	214.8
empty *C*	8	0	4.35	7.52	7.07	90°	90°	90°	231.0
1 CO_2 *C*	8	1	4.50	8.23	6.85	85°	90°	90°	252.8
2 CO_2 *C*	8	2	4.51	8.84	7.41	90°	92°	90°	295.0
3 CO_2 *C*	8	3	4.58	9.76	7.19	87°	91°	93°	320.6
4 CO_2 *C*	8	4	4.54	10.58	7.58	90°	92°	90°	363.8

[a]Experimental value from Amos et al.,[17] T = 260 K, P = 0.4 GPa.

phase transition, and the harmonic vibrational modes and frequencies. The planetary implications of the high pressure hydrate system in the Jovian icy moon Ganymede are discussed in Section 4. The article ends with a brief summary of our findings and conclusions.

2. COMPUTATIONAL DETAILS

We have performed computational simulations with the Quantum Espresso[18] suite of programs that works with pseudopotentials. Our computations are ab initio and use density functional theory (DFT)[19,20] under periodic boundary conditions. We used the projector augmented wave (PAW) pseudopotentials[21] for every atom. We employed the PW86PBE functional.[22−24] To take into account dispersion interactions we included the XMD method.[25−28] This methodology has been proven to be accurate to study both equilibrium and nonequilibrium geometries in gas and condensed phases.[29,30] Our XMD parameters were[30] $a1$ = 0.136 and $a2$ = 3.178 Å.

We used a 60 Ry cutoff energy for the planewaves, ensuring convergence of the total energy. We employed a 2 × 2 × 2 Monkhorst−Pack grid.[31] The convergence for the self consistent field (SCF) method was 10^{-8} Rydberg. Full (atomic positions and lattice parameters) geometry optimizations were performed using the Broayden−Fletcher−Goldfarb−Shanno (BFGS)[32] algorithm. Equations of state (EOS) were computed using the Gibbs2 program.[33−35]

The noncovalent interactions (NCI) analysis were performed using the reduced density gradient (RDG)[36] scalar field as implemented in the NCIPLOT program,[37] included in the CRITIC2 code.[38] Vibrational computations were performed at the Γ point using density functional perturbation theory (DFPT),[39] included in the Quantum Espresso suite. All the structure drawings were done with the program VESTA.[40]

3. RESULTS AND DISCUSSION

In recent years there have been several proposals for potential structures to which the CO_2 clathrate *sI* phase could transition into under increasing pressure. Three plausible candidates are analyzed here. We will mainly focus our discussion on the most likely one according to our calculations, the one thermodynamically stable at high pressure. The three candidates are (i) a hydrate similar to the methane hydrate MH-III phase,[13] (ii) the so-called C_0 structure that had only been previously

https://dx.doi.org/10.1021/acsearthspacechem.0c00198
ACS Earth Space Chem. XXXX, XXX, XXX−XXX

observed in hydrogen hydrate,[17] and (iii) a possible alternative related to C_0 that was found close in energy in computational studies of H_2 hydrates.[41] In what follows, we refer to these structures as filled ice structures *A*, *B*, and *C*, respectively. Figure 1 shows the optimized unit cells of the three candidates.

In all these cases, the aqueous framework structure no longer contains cages but channels running through the crystal. For this reason, these structures are usually called nonclathrate or postclathrate. Throughout this whole section, we frequently resort to the weak interactions between host−host, host−guest, and guest−guest molecules to support, interpret, and explain our results. Technical and detailed information on these so-called noncovalent interactions (NCI) are provided separately in the Supporting Information (SI) file.

3.1. Alternative High Pressure Structures. In Table 1 we present the optimized lattice parameters for each of the three potential candidates studied both with and without CO_2 molecules inside the water framework. The maximum gas occupation goes up to a 1:2 ratio between CO_2 and water molecules. In the SI file, the calculated optimized positions of all the atoms for each structure are collected.

As seen in Table 1, *A* and *C* structures are both orthorhombic, whereas *B* has a hexagonal cell. For the orthorhombic lattices *A* and *C*, the number of water molecules in their unit cells is 8 and the maximum number of guest molecules that can be accommodated is 4. In the case of the hexagonal structure (*B*), the number of water molecules per unit cell is 6 and can host up to 3 guest molecules. As we previously mentioned, the three structures no longer present cages, but have channels where CO_2 molecules are always located displaying an oblique disposition with respect to each other and complying with the following general rule: the more the space they have in the channel, the more perpendicular they will be oriented relative to each other. This configuration is reminiscent of the organization that occurs in the cubic structure of the ice CO_2−I phase, and tells us that some interaction is taking place between the guest molecules. This molecular configuration does not occur in the low pressure phase of this CO_2 hydrate.

The water molecules are oriented following the rules of water ice, with a tetrahedral geometry around oxygen atoms: two nearby hydrogen atoms linked by covalent bonds and two hydrogen atoms far linked by hydrogen bonding. Keeping in mind that, due to the multiple possible configurations of water molecules, these systems have disorder of protons, we choose to place the protons in the positions that guarantee a null total dipole moment of the cell, whereas at the same time we try to keep as far as possible the symmetry of each structure.

In the case of the structure *A*, optimizations were performed to find the lowest energy configuration among the structures that produced a zero dipole moment, since the placement of the hydrogen atoms yield a total breakdown of symmetry reducing it to *P*1. For *B*, a spatial symmetry was found that allowed to place all the hydrogen atoms without disorder. The skeleton of water molecules in the structure follows the $P3_2$ space group, which cancels the total dipole moment of the cell. By including the guest molecules, the structure loses its point symmetry and its space group is reduced to *P*1. In the case of *C*, we start from the skeleton already obtained in a previous study carried out for hydrogen hydrates that also displays a *P*1 symmetry.[41]

CO_2 molecules enter into the water framework up to reach the maximum theoretical capacity inducing distortions in the geometry of the cells with respect to their ideal symmetry. Whether major or minor drastic changes occur primarily depends on the host water structure. For example, in the case of the *A* lattice, an initial contraction due to the attractive dispersion interaction between the guest molecule and the water framework is followed by an expansion of the structure as more CO_2 molecules are introduced in order to accommodate them within the lattice.

In the case of *B*, after the first guest molecule goes inside the structure, there is a contraction of the *a* and *b* lattice parameters, whereas the parameter *c* grows significantly. This is because the channel where the molecules of CO_2 are hosted is oriented along the *c* axis of the unit cell in a helical arrangement. This can be seen more clearly in Figure 2

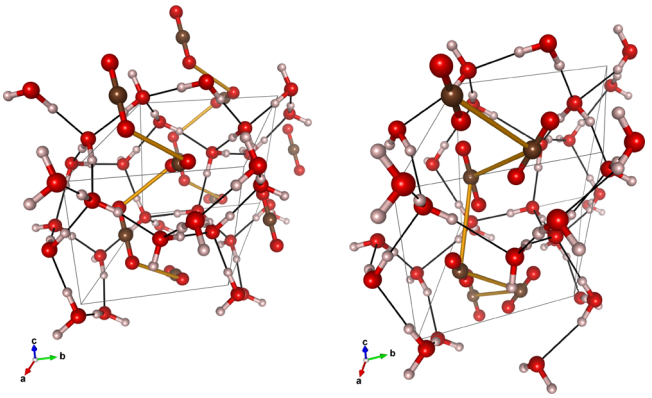

Figure 2. Images of the *B* structure highlighting the helical symmetry in the channel where 2 (left) and 3 (right) CO_2 molecules are hosted.

where oxygen atoms of different CO_2 molecules have been connected to guide and mark the helical configuration of the channel. Induced by the first CO_2 guest molecule, the *B* structure also suffers a deformation of its unit cell angles that is progressively removed by introducing more CO_2 molecules. *B* is the structure determined by neutron diffraction.[17] It is currently accepted after demonstrating a better fit to the experimental diffraction data than the proposed alternative structure *A*. Interestingly enough, our *B* structure with 2 CO_2 molecules in the unit cell is in good agreement with the lattice parameters of the experimental accepted structure.

Finally, in the *C* structure the parameter *b* grows considerably, suffering a change of about 3 Å as CO_2 molecules are progressively accommodated in the unit cell. Also, in this case no contraction is seen after the first guest molecule is introduced. This fact clearly tells us that the water framework is more compact in this structure than in the other two cases. The inclusion of guest molecules forces from the beginning an expansion of the structure leading to an overall loss of the system stability.

In addition to the structures fully saturated with host molecules, we studied possible intermediate states, in which we fill the host structures with CO_2 molecules, one by one, until the saturation is reached. We found that the lowest energy structure is obtained in the *B* structure, which coincides with the most recent structural determination of the high pressure phase of CO_2@H_2O.[17] The results we present below are for this *B* structure that we will call from now on phase C_0.

3.2. C_0 EOS. The pressure behavior of the experimentally observed C_0 high pressure phase with different CO_2 occupations is worth to be computationally simulated due to

https://dx.doi.org/10.1021/acsearthspacechem.0c00198
ACS Earth Space Chem. XXXX, XXX, XXX−XXX

the implications that the density of the CO_2@H_2O system has on different planetary conditions. The static (zero temperature and zero point vibrations neglected) Vinet EOS parameters for the empty structure and with up to 3 CO_2 guest molecules are collected in Table 2. The Vinet EOS has the following functional form:

Table 2. Vinet EOS Parameters for the High Pressure C_0 Polymorph of CO_2@H_2O Empty and with 1, 2, and 3 CO_2 Molecules

structure	V_0 (Å^3)	B_0 (GPa)	B_0
C_0 empty	1370.6	14.05	3.92
C_0 1 CO_2	1399.1	17.55	2.04
C_0 2 CO_2	1528.8	15.67	5.60
C_0 3 CO_2	1969.8	9.86	6.77

$$P(V) = 3B_0\left(\frac{1-x}{x^2}\right)e^{3/2(B_0'-1)(1-x)} \qquad x = \left(\frac{V}{V_0}\right)^{1/3} \tag{1}$$

where V_0, B_0, and B_0' are, respectively, the volume, the bulk modulus, and its pressure derivative, all evaluated at zero pressure. Notice that B_0 is the inverse of the compressibility. It is clear that as gas saturation is achieved the structure expands and the compressibility increases. This last result might be seen as counterintuitive if one resorts to steric effects dominating the saturated system. However, a simple argument based on the weakening of the H-bonding as the cell increases in size explains why the saturated structure is the most compressible one. This will be corroborated later in the discussion of phase stability where the 3-molecule CO_2 structure is found to be the least energetically favorable of all.

Experimentally, the density of the CO_2@H_2O high pressure phase is found with a value of 1.5 g/cm^3 at a pressure close to 0.5 GPa.[17] Since neutron diffraction experiments were conducted on deuterated CO_2@D_2O hydrates, we have evaluated the density pressure curves of Figure 3 taking into account this fact. The increase of the number of CO_2 molecules in the water framework yields two opposite effects on the density. On the one hand, it increases the mass per formula unit. On the other hand, there is also an increasing in the unit cell that leads to a decreasing in the mass density. This effect is more intense as pressure is applied as we have seen in the analysis of the EOS parameters. For example, the overexpansion of the structure with 3 CO_2 molecules makes it less dense than the structure with two CO_2 molecules (see Figure 3). If we want to match the observed density then an interpolated value with an occupation of 1.69 CO_2 molecules per unit cell is necessary. This value is in very good agreement with the experimental study of Amos et al.[17]

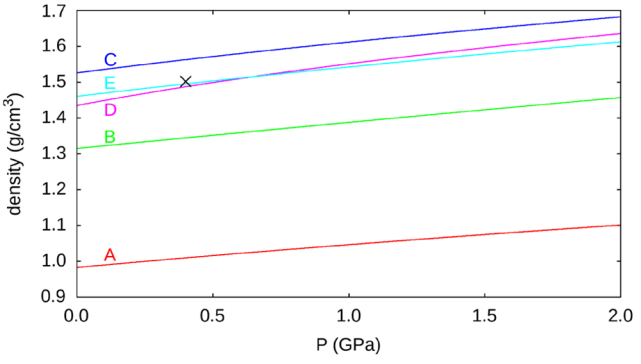

Figure 3. Density variation of the C_0 structure with respect to pressure calculated using deuterated water. A is the Empty C_0 structure, B is 1CO_2−C_0, C is 2CO_2−C_0, D is 3CO_2−C_0, E is 1.69CO_2−C_0, the experimental occupation. The cross is the experimental datum obtained from Amos et al.[17]

3.3. Relative Stability of CO_2@H_2O Polymorphs at High Pressure. Once the C_0 structures with different CO_2 occupancies were found and characterized, it is possible to determine which pressure-induced phase transitions can occur between the low and high pressure structures. We follow a static strategy avoiding the calculation of more complex thermal contributions. These should consider anharmonic effects too and are beyond our computational scheme. Whereas we are aware of the importance of thermal effects in each polymorph, we understand that the evaluation of enthalpy (H) instead of Gibbs energy (G) does not introduce meaningful deviations as far as relative energies and transition pressures are concerned.

Two additional considerations have to be taken into account due to the different H_2O:CO_2 ratios of these polymorphs. First, we need to introduce the equation of state of solid CO_2. The second one requires the calculation of the stoichiometric coefficients involved in the chemical equations associated with the transformations. The details on the calculation of the relative enthalpies of the systems are included in the SI.

Once the relationships are obtained, they can be drawn as a function of pressure with the aim at finding the stable phase at each pressure. We will consider a pressure range from 0 to 2 GPa, which is well described by the calculated EOS. In Figure 4, the variations with pressure of the enthalpy of the three different CO_2@H_2O systems are plotted. The figure has not included the curve of the empty hydrate since it has a higher energy than the other hydrates and does not provide extra information.

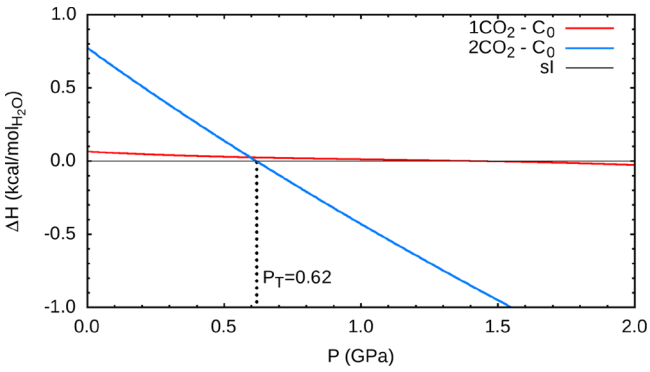

Figure 4. Enthalpy versus pressure for CO_2 hydrates involved in the pressure induced phase transition.

We can see that the C_0 structure with 2 CO_2 molecules becomes more favorable than the low pressure clathrate *sI* at a transition pressure of P_T = 0.62 GPa. Our computed value successfully reproduces previous experimental results[4,42] that observe the phase transition around 0.7 GPa. This is our first result to highlight concerning phase stability. Second, it is interesting to notice that the curve of the C_0 structure with 1 CO_2 molecule shows similar enthalpy as the *sI* phase in all the pressure range studied. Up to around 1.4 GPa it is higher, and

https://dx.doi.org/10.1021/acsearthspacechem.0c00198
ACS Earth Space Chem. XXXX, XXX, XXX−XXX

from this value to 2.0 GPa the enthalpy of the C_0 phase with one CO_2 molecule is lower than that of the *sI* phase.

Supported by the close stability of these two phases and the structural similarity between the C_0 lattices with one and two CO_2 molecules, it is appealing to propose a scenario in which the CO_2@H_2O system could transit to the high pressure phase in a compression cycle and, when performing the expansion, does not return to the *sI* phase but keeps its C_0 structure, releasing part of the CO_2 contained in its nonclathrate water framework. CO_2 degassing would not be a difficult process provided CO_2 molecules could easily diffuse through the channels of the C_0 structure. Confirmation of this fact is given below and further underpins our proposal of intermediate high pressure structures with partial CO_2 occupancies, which are totally compatible with those experimentally observed by Amos et al.[17] It is therefore reasonable to state that the real situation will be one in which there is a great structural disorder of the CO_2 molecules moving almost without restriction along the channels of the C_0 nonclathrate structure.

Verification of the quasi-free translation of CO_2 molecules along the open channels of the C_0 structure is provided by the analysis of the results displayed in Figure 5. The value of the

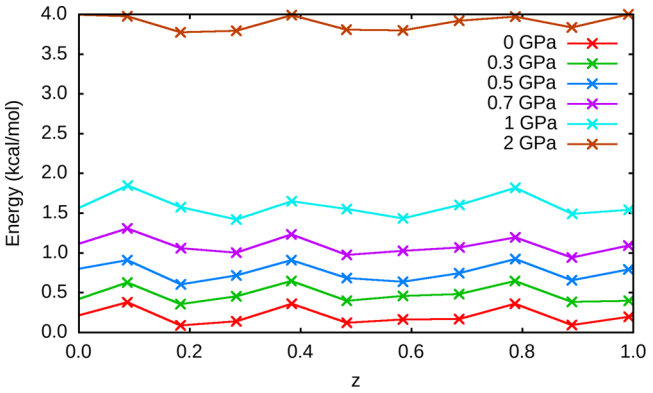

Figure 5. Relative energies of the C_0 phase of the CO_2@H_2O hydrate according to the position of the CO_2 molecule along the *c* axis.

carbon fractional coordinate on the *c* axis is used as the abscissa in the representation of the calculated energies of the CO_2@H_2O system with one CO_2 molecule in the C_0 structure. The energy barriers associated with this molecular translation are computed as the energy difference between minima and maxima of the curves. The study was carried out at different pressures to check whether compression of the system affects energy barriers. In all cases, values as low as around 0.5 kcal/mol were obtained. However, the movement is slightly constrained within the channel since it is not linear with the direction of the *c* axis. The CO_2 molecule rotates as it progresses upward along the helical axis that governs the symmetry of the skeleton of the water framework. Different frames of the helical movement of the CO_2 molecule around the *c* axis are displayed in the SI file. This unique behavior would allow the diffusion of CO_2 through a macroscopic layer of a planetary body composed by this hydrate, which could even be considered a semipermeable barrier for this type of gas.

3.4. Vibrations in the High Pressure C_0 Phase of CO_2@H_2O. Vibrational frequencies obtained from the calculation of the crystalline phonons at the Γ point are discussed here. The calculated values can be directly compared with the vibrational frequencies obtained in infrared and Raman experiments. Besides the three frequencies close to zero associated with the three acoustic modes of the crystal, the existence of modes with imaginary frequencies allows us to identify dynamic instabilities in crystalline lattices. In the C_0 structure with 3 CO_2 molecules this situation occurs as revealed by the appearance of three imaginary frequencies. This fact is very likely related to the results discussed in the previous subsection, in which we highlighted a too large unit cell size and the excessive open structure for this degree of CO_2 occupation. In C_0 hydrates with one and two CO_2 molecules, all phonons present positive frequencies and are dynamically stable. Representative values at the Γ point are collected in Table 3.

If we look first at the stretching modes of the CO_2 molecule we observe a slight pressure dependency with a blue shift of the frequencies. This is related to a compression of the C═O double bond which leads to an increase in its force constant. Another interesting finding is that, in the case of the symmetrical stretching, an increase in frequency occurs when including one more molecule of CO_2. In the case of the antisymmetric stretching, a mode splitting effect occurs induced by the second CO_2 molecule: one frequency appears at a lower value and another at a higher value than the value found just with one guest molecule. This can be related to the interaction that is occurring between the two CO_2 molecules experiencing this antisymmetric mode. In the low-frequency mode, oxygen atoms of the two molecules move in the same direction, the intermolecular distance is hardly modified, and, therefore, the frequency varies little with respect to the case with a single CO_2 molecule. Regarding the high frequency value of the interval, the movement of the two CO_2 molecules is in opposite directions so that the intermolecular distance will vary a lot, creating a potential energy curve with a greater curvature and therefore a higher frequency.

If we go on to analyze the vibrational modes associated with water, we first see an equivalent behavior observed in low pressure clathrates: with increasing pressure the stretching modes soften because we are bringing the water molecules

Table 3. Frequencies Calculated in cm^{-1} of the Most Characteristic Modes of Water and CO_2 in the High Pressure C_0 Structure with One and Two Guest Molecules[a]

	$1CO_2$–C_0			$2CO_2$–C_0		
P(GPa)	0	0.5	1.0	0	0.5	1.0
SS CO_2	1315	1316	1317	1319–1321	1321–1323	1322–1324
AS CO_2	2330	2331	2334	2324–2353	2327–2357	2328–2359
B H_2O	1614–1691	1613–1693	1612–1695	1623–1686	1623–1689	1623–1692
S H_2O	3015–3349	2983–3333	2945–3314	3137–3400	3102–3380	3078–3367

[a]SS = symmetric stretching, AS = antisymmetric stretching, B = bending, S = stretching.

https://dx.doi.org/10.1021/acsearthspacechem.0c00198
ACS Earth Space Chem. XXXX, XXX, XXX–XXX

closer to each other, producing an increase in the strength of the hydrogen bonds and a weakening of covalent O−H bonds. We note that by introducing a CO_2 molecule into the system the frequencies shift to blue. When introducing a new CO_2 molecule the volume of the cell increases, as we have quantified previously, so the water molecules move away from each other weakening intermolecular hydrogen bonds. This makes the covalent O−H bonds to reinforce, thereby increasing their frequency. The fact that these shifts in the water- and CO_2-localized frequencies are within an interval of several cm^{-1} makes it worthy to be analyzed and reported.

4. PLANETARY IMPLICATIONS

Among the planetary bodies in the solar system, Ganymede is proposed to have CO_2 in its composition[43,44] and is the one where the thermodynamic conditions to form high pressure CO_2 hydrates can be achieved. It has a deep global ocean where it is estimated that more than 1 GPa of pressure is reached at the water/rock interface.

Depending on the thermal profile of Ganymede we could find one of two possible subsurface ocean scenarios. A warm thermal profile would melt all the subsurface ocean up to where the pressure is high enough to crystallize into Ice VI.[45,46] The colder profile could result in a "cake"-like structure.[47,49,50] To clarify, we include in Figure 6 the proposed phase diagram of the compounds related to Ganymede and the moon's proposed thermal profiles.

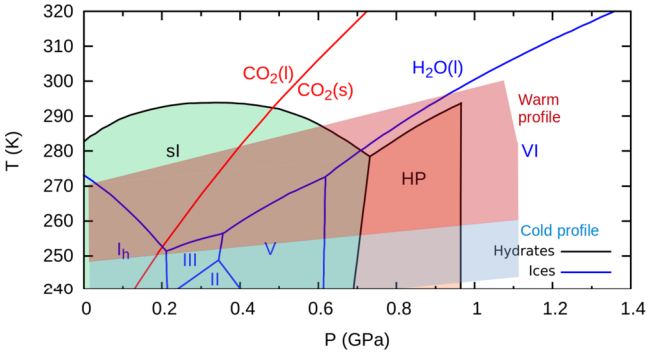

Figure 6. Pressure−temperature CO_2−H_2O phase diagram. Adapted from Bollengier et al.[4] and Sohl et al.[45]

Calculating the densities of these systems and comparing them with the different densities of water ice and high pressure brines, we can estimate the position where CO_2 hydrates would occupy in a differentiated planetary structure. In Table 4 we present relevant numbers related to these densities. It is important to take into account that our calculations have not taken into account the thermal expansion, so the real solids would have slightly lower densities than presented.

Table 4. Range of Densities between 0 and 1 GPa[a]

subs. (exp.)	dens. (g/mL)	subs. (comp.)	dens. (g/mL)
Ice Ih	0.92−0.95	$6CO_2$−*sI*	1.12−1.19
Ice III	1.12−1.23	$8CO_2$−*sI*	1.21−1.28
Ice V	1.17−1.30	$1CO_2$−C_0	1.22−1.29
Ice VI	1.39−1.45	$1.69CO_2$−C_0	1.37−1.45
water/brines	1.00−1.40	$2CO_2$−C_0	1.44−1.52

[a]For water ice, data were taken from ref 48. Data from brines were taken from refs 46, 47. The *sI* EOS was reported by us in ref 14.

Considering that there is enough CO_2 to form hydrates in the planetary body from degasification of primordial rocks and the ice accretion from cometary-like bodies, some structural scenarios are suggested attending to the different densities of the substances. We can see that the ice Ih is clearly the lightest and will be the main component of the external crust. Then we might have some very dilute brine or a partially occupied *sI* clathrate. As we go deeper into the moon we would find clathrates with higher occupation (as pressure also favors occupation). Depending on the thermal profile we could now find a deep brine ocean or a series of layers of ices and brines. Finally, at the rock water interfaces we would find ice VI and CO_2 high pressure hydrate. They seem to have very similar densities depending on the occupation of the hydrate. We can expect a layer of high pressure clathrate in contact with the rock water interface. Brines of different concentrations have a wide range of densities with pressure, ranging from 1.00 g/mL (pure water at 1 bar) to 1.40 g/mL (2.5 mol/kg Mg_2SO_4). This means that depending on the ocean salinity, the buoyancy of the systems might differ. In Figure 7 we represent the expected regions of appearance of CO_2 hydrates inside Ganymede in two different models previously proposed.[46,47] Not all of the layers are necessarily present.

As we have described in previous sections, the C_0 phase allows the translation of its guest molecule through its channels. This would mean that we could find a permeable solid barrier through which volatiles could pass from the bottom of the barrier to an upper part of the moon following concentration gradients. If the CO_2−C_0 layer is formed from the degassing of the silicate rock during the body differentiation, and the guest molecules move upward due to the crystal permeability, two scenarios are possible: (1) If the CO_2−C_0 layer is in direct contact with the ocean, CO_2 would be delivered to the brine, where it can be dissolved or form CO_2−*sI* (depending on the temperature gradient). The secondary hydrate could ascend to the top of the liquid layer. In this case, the initial CO_2−C_0 layer would be consumed with time, leaving an ice VI layer in contact with the ocean. (2) If the CO_2−C_0 layer is in contact with a formerly ice VI layer with low permeability, the volatile would be blocked at the interface and would not reach the ocean. The accumulation of CO_2 molecules would increase the density of the upper part of the layer, which could produce instabilities with respect to the bottom and potentially overturns. Multiple layers of ice phases would obstruct the ascending of volatiles. Otherwise, CO_2 can come from the cometary input, so the CO_2−*sI* formation at the upper layer would be favored.

5. CONCLUSION

Using ab initio DFT computations we have deepened the knowledge of the high pressure phase of the CO_2 hydrate. We have provided a thermodynamic estimation of the transition pressure from the *sI* low pressure phase to the C_0 high pressure phase with a value of 0.62 GPa. The computed stable HP structure shows a good agreement with the experimental one and confirms a CO_2 occupancy closer to two molecules in the unit cell. We have also calculated the vibrational properties of this HP phase and used them to analyze the effects of the intermolecular interactions in this system. We have found a possible translation movement of the CO_2 through the structure that could allow the interchange of volatiles across

https://dx.doi.org/10.1021/acsearthspacechem.0c00198
ACS Earth Space Chem. XXXX, XXX, XXX−XXX

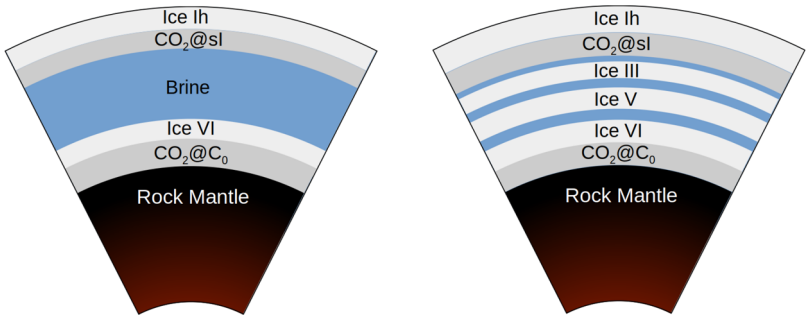

Figure 7. Ganymede's proposed internal differentiation with the CO_2 hydrates' gravitational stable position included. Not all of the layers are necessarily present. Left: Warm thermal profile. Right: Cold thermal profile.

a solid icy barrier with the planetary implications that that has, as allowing carbon rich oceans even though they are isolated by icy barriers. Taking into account its density, very similar to ice VI, and comparing it with other substances we can estimate its naturally occurring zone at the bottom of the ocean inside a giant frozen world as Ganymede.

■ ASSOCIATED CONTENT

Supporting Information

The Supporting Information is available free of charge at https://pubs.acs.org/doi/10.1021/acsearthspacechem.0c00198.

Details on the calculation of the relative enthalpies of the different structures; Noncovalent interactions analysis; Optimized geometries of all the atoms in the different structures; Snapshots of CO_2 movement through the channel (PDF)

■ AUTHOR INFORMATION

Corresponding Author

Fernando Izquierdo-Ruiz − *MALTA-Consolider Team and Departamento de Química Física, Universidad Complutense de Madrid, 28040 Madrid, Spain;* orcid.org/0000-0001-7237-4720; Email: fizqru@gmail.com

Authors

J. Manuel Recio − *MALTA-Consolider Team, Universidad Complutense de Madrid, 28040 Madrid, Spain; Departamento de Química Física y Analítica, Universidad de Oviedo, 33003 Oviedo, Asturias, Spain;* orcid.org/0000-0002-3182-7508

Olga Prieto-Ballesteros − *MALTA-Consolider Team, Universidad Complutense de Madrid, 28040 Madrid, Spain; Departamento de Planetología y Habitabilidad, Centro de Astrobiología, 28850 Torrejón de Ardoz, Spain*

Complete contact information is available at: https://pubs.acs.org/10.1021/acsearthspacechem.0c00198

Notes

The authors declare no competing financial interest.

■ ACKNOWLEDGMENTS

Financial support from MCIU, Principado de Asturias-FICYT, and FEDER (projects PGC2018-094814−B-C22, FC-GRU-PIN-IDI/2018/000177, RED2018-102612-T) are gratefully acknowledged. We would like to thank the MALTA-Consolider computational facilities for providing us the computational resources. OPB would like to thank the Spanish MINECO projects ESP2017-89053-C2-1-P, RED2018-102612-T, and the AEI project MDM-2017-0737 Unidad de Excelencia "María de Maeztu".

■ REFERENCES

(1) Hussmann, H.; Sohl, F.; Spohn, T. Subsurface oceans and deep interiors of medium-sized outer planet satellites and large trans-neptunian objects. *Icarus* **2006**, *185*, 258−273.

(2) Fortes, A. D. Titan's internal structure and the evolutionary consequences. *Planet. Space Sci.* **2012**, *60*, 10−17.

(3) Izquierdo-Ruiz, F.; Méndez, A. S. J.; Prieto-Ballesteros, O.; Recio, J. M. Study of high pressure carbon dioxide clathrates hydrates on Ganymede. *European Planetary Science Congress* 2015; Sep 27 to Oct 2, 2015, Nantes, France; EPSC2015−849.

(4) Bollengier, O.; Choukroun, M.; Grasset, O.; Le Menn, E.; Bellino, G.; Morizet, Y.; Bezacier, L.; Oancea, A.; Taffin, C.; Tobie, G. Phase equilibria in the H2O−CO2 system between 250−330 K and 0−1.7 GPa: Stability of the CO2 hydrates and H2O-ice VI at CO2 saturation. *Geochim. Cosmochim. Acta* **2013**, *119*, 322−339.

(5) Henning, R. W.; Schultz, A. J.; Thieu, V.; Halpern, Y. Neutron diffraction studies of CO2 clathrate hydrate: Formation from deuterated ice. *J. Phys. Chem. A* **2000**, *104*, 5066−5071.

(6) Udachin, K. A.; Ratcliffe, C. I.; Ripmeester, J. A. Structure, composition, and thermal expansion of CO2 hydrate from single crystal X-ray diffraction measurements. *J. Phys. Chem. B* **2001**, *105*, 4200−4204.

(7) Loveday, J.; Nelmes, R.; Guthrie, M.; Belmonte, S.; Allan, D.; Klug, D.; Tse, J.; Handa, Y. Stable methane hydrate above 2 GPa and the source of Titan's atmospheric methane. *Nature* **2001**, *410*, 661−663.

(8) Tulk, C. A.; Klug, D. D.; dos Santos, A. M.; Karotis, G.; Guthrie, M.; Molaison, J. J.; Pradhan, N. Cage occupancies in the high pressure structure H methane hydrate: A neutron diffraction study. *J. Chem. Phys.* **2012**, *136*, 054502.

(9) Izquierdo-Ruiz, F.; Otero-de-la Roza, A.; Contreras-García, J.; Menéndez, J.; Prieto-Ballesteros, O.; Recio, J. Guest−host interactions in gas clathrate hydrates under pressure. *High Pressure Res.* **2015**, *35*, 49−56.

(10) Román-Pérez, G.; Moaied, M.; Soler, J. M.; Yndurain, F. Stability, adsorption, and diffusion of CH4, CO2, and H2 in clathrate hydrates. *Phys. Rev. Lett.* **2010**, *105*, 145901.

(11) Kumar, P.; Sathyamurthy, N. Theoretical studies of host−guest interaction in gas hydrates. *J. Phys. Chem. A* **2011**, *115*, 14276−14281.

(12) Loveday, J.; Nelmes, R. High-pressure gas hydrates. *Phys. Chem. Chem. Phys.* **2008**, *10*, 937−950.

(13) Tulk, C. A.; Machida, S.; Klug, D. D.; Lu, H.; Guthrie, M.; Molaison, J. J. The structure of CO2 hydrate between 0.7 and 1.0 GPa. *J. Chem. Phys.* **2014**, *141*, 174503.

(14) Izquierdo-Ruiz, F.; Otero-De-La-Roza, A.; Contreras-García, J.; Prieto-Ballesteros, O.; Recio, J. M. Effects of the CO2 guest molecule on the sI clathrate hydrate structure. *Materials* **2016**, *9*, 777.

(15) Falenty, A.; Salamatin, A.; Kuhs, W. Kinetics of CO2-hydrate formation from ice powders: Data summary and modeling extended to low temperatures. *J. Phys. Chem. C* **2013**, *117*, 8443−8457.

https://dx.doi.org/10.1021/acsearthspacechem.0c00198
ACS Earth Space Chem. XXXX, XXX, XXX−XXX

(16) Ambuehl, D.; Madden, M. E. CO2 hydrate formation and dissociation rates: Application to Mars. *Icarus* **2014**, *234*, 45−52.
(17) Amos, D. M.; Donnelly, M.-E.; Teeratchanan, P.; Bull, C. L.; Falenty, A.; Kuhs, W. F.; Hermann, A.; Loveday, J. S. A Chiral Gas−Hydrate Structure Common to the Carbon Dioxide−Water and Hydrogen−Water Systems. *J. Phys. Chem. Lett.* **2017**, *8*, 4295−4299.
(18) Giannozzi, P.; Baroni, S.; Bonini, N.; Calandra, M.; Car, R.; Cavazzoni, C.; Ceresoli, D.; Chiarotti, G. L.; Cococcioni, M.; Dabo, I.; et al. QUANTUM ESPRESSO: a modular and open-source software project for quantum simulations of materials. *J. Phys.: Condens. Matter* **2009**, *21*, 395502.
(19) Hohenberg, P.; Kohn, W. Inhomogeneous electron gas. *Phys. Rev.* **1964**, *136*, B864−B871.
(20) Kohn, W.; Sham, L. J. Self-consistent equations including exchange and correlation effects. *Phys. Rev.* **1965**, *140*, A1133−A1138.
(21) Kresse, G.; Joubert, D. From ultrasoft pseudopotentials to the projector augmented-wave method. *Phys. Rev. B: Condens. Matter Mater. Phys.* **1999**, *59*, 1758−1775.
(22) Perdew, J. P.; Yue, W. Accurate and simple density functional for the electronic exchange energy: Generalized gradient approximation. *Phys. Rev. B: Condens. Matter Mater. Phys.* **1986**, *33*, 8800−8802.
(23) Perdew, J. P.; Burke, K.; Ernzerhof, M. Generalized gradient approximation made simple. *Phys. Rev. Lett.* **1996**, *77*, 3865−3868.
(24) Perdew, J. P.; Burke, K.; Ernzerhof, M. Generalized Gradient Approximation Made Simple. *Phys. Rev. Lett.* **1996**, *77*, 3865; *Phys. Rev. Lett.* **1997**, *78*, 1396−1396.
(25) Becke, A. D.; Johnson, E. R. A density-functional model of the dispersion interaction. *J. Chem. Phys.* **2005**, *123*, 154101.
(26) Johnson, E. R.; Becke, A. D. A post-Hartree-Fock model of intermolecular interactions: Inclusion of higher-order corrections. *J. Chem. Phys.* **2006**, *124*, 174104.
(27) Becke, A. D.; Johnson, E. R. Exchange-hole dipole moment and the dispersion interaction revisited. *J. Chem. Phys.* **2007**, *127*, 154108.
(28) Arabi, A. A.; Becke, A. D. Assessment of the PW86+ PBE+ XDM density functional on van der Waals complexes at non-equilibrium geometries. *J. Chem. Phys.* **2012**, *137*, 014104.
(29) Otero-De-La-Roza, A.; Johnson, E. R. Non-covalent interactions and thermochemistry using XDM-corrected hybrid and range-separated hybrid density functionals. *J. Chem. Phys.* **2013**, *138*, 204109.
(30) Otero-De-La-Roza, A.; Johnson, E. R. Van der Waals interactions in solids using the exchange-hole dipole moment model. *J. Chem. Phys.* **2012**, *136*, 174109.
(31) Monkhorst, H. J.; Pack, J. D. Special points for Brillouin-zone integrations. *Phys. Rev. B* **1976**, *13*, 5188−5192.
(32) Fletcher, R. *Practical Methods of Optimization*; John Wiley & Sons, 1980.
(33) Blanco, M.; Francisco, E.; Luana, V. GIBBS: isothermal-isobaric thermodynamics of solids from energy curves using a quasi-harmonic Debye model. *Comput. Phys. Commun.* **2004**, *158*, 57−72.
(34) Otero-de-la Roza, A.; Luaña, V. Gibbs2: A new version of the quasi-harmonic model code. I. Robust treatment of the static data. *Comput. Phys. Commun.* **2011**, *182*, 1708−1720.
(35) Otero-de-la Roza, A.; Abbasi-Pérez, D.; Luaña, V. Gibbs2: A new version of the quasiharmonic model code. II. Models for solid-state thermodynamics, features and implementation. *Comput. Phys. Commun.* **2011**, *182*, 2232−2248.
(36) Johnson, E. R.; Keinan, S.; Mori-Sánchez, P.; Contreras-García, J.; Cohen, A. J.; Yang, W. Revealing noncovalent interactions. *J. Am. Chem. Soc.* **2010**, *132*, 6498−6506.
(37) Contreras-García, J.; Johnson, E. R.; Keinan, S.; Chaudret, R.; Piquemal, J.-P.; Beratan, D. N.; Yang, W. NCIPLOT: a program for plotting noncovalent interaction regions. *J. Chem. Theory Comput.* **2011**, *7*, 625−632.
(38) Otero-de-la Roza, A.; Johnson, E. R.; Luaña, V. Critic2: A program for real-space analysis of quantum chemical interactions in solids. *Comput. Phys. Commun.* **2014**, *185*, 1007−1018.
(39) Baroni, S.; De Gironcoli, S.; Dal Corso, A.; Giannozzi, P. Phonons and related crystal properties from density-functional perturbation theory. *Rev. Mod. Phys.* **2001**, *73*, 515−562.
(40) Momma, K.; Izumi, F. *VESTA3* for three-dimensional visualization of crystal, volumetric and morphology data. *J. Appl. Crystallogr.* **2011**, *44*, 1272−1276.
(41) Qian, G.-R.; Lyakhov, A. O.; Zhu, Q.; Oganov, A. R.; Dong, X. Novel hydrogen hydrate structures under pressure. *Sci. Rep.* **2015**, *4*, 5606.
(42) Hirai, H.; Komatsu, K.; Honda, M.; Kawamura, T.; Yamamoto, Y.; Yagi, T. Phase changes of CO2 hydrate under high pressure and low temperature. *J. Chem. Phys.* **2010**, *133*, 124511.
(43) Dalton, J. Spectroscopy of icy moon surface materials. *Space Sci. Rev.* **2010**, *153*, 219−247.
(44) Mousis, O.; Alibert, Y. Modeling the Jovian subnebula-II. Composition of regular satellite ices. *Astron. Astrophys.* **2006**, *448*, 771−778.
(45) Sohl, F.; Choukroun, M.; Kargel, J.; Kimura, J.; Pappalardo, R.; Vance, S.; Zolotov, M. Subsurface water oceans on icy satellites: Chemical composition and exchange processes. *Space Sci. Rev.* **2010**, *153*, 485−510.
(46) Vance, S.; Bouffard, M.; Choukroun, M.; Sotin, C. Ganymede's internal structure including thermodynamics of magnesium sulfate oceans in contact with ice. *Planet. Space Sci.* **2014**, *96*, 62−70.
(47) Vance, S.; Brown, J. M. Thermodynamic properties of aqueous MgSO4 to 800 MPa at temperatures from −20 to 100° C and concentrations to 2.5 mol kg^{-1} from sound speeds, with applications to icy world oceans. *Geochim. Cosmochim. Acta* **2013**, *110*, 176−189.
(48) Choukroun, M.; Grasset, O. Thermodynamic data and modeling of the water and ammonia-water phase diagrams up to 2.2 GPa for planetary geophysics. *J. Chem. Phys.* **2010**, *133*, 144502.
(49) Simon, A.; Peters, K. Single-crystal refinement of the structure of carbon dioxide. *Acta Crystallogr., Sect. B: Struct. Crystallogr. Cryst. Chem.* **1980**, *36*, 2750−2751.
(50) Contreras-García, J.; Boto, R. A.; Izquierdo-Ruiz, F.; Reva, I.; Woller, T.; Alonso, M. A benchmark for the non-covalent interaction (NCI) index or... is it really all in the geometry? *Theor. Chem. Acc.* **2016**, *135*, 242.

https://dx.doi.org/10.1021/acsearthspacechem.0c00198
ACS Earth Space Chem. XXXX, XXX, XXX−XXX